# Impact of Angiogenesis Inhibition by Sunitinib on Tumor Distribution of Temozolomide

Qingyu Zhou, Ping Guo, and James M. Gallo

**Abstract**

**Purpose:** As combination chemotherapy of antiangiogenic agents with conventional chemotherapeutic drugs continues to evolve, an understanding of the pharmacokinetic and pharmacodynamic variables associated with optimal treatment is needed. Thus, the effect of the multitargeted tyrosine kinase inhibitor sunitinib on tumor distribution of temozolomide was investigated to evaluate conditions for optimal combination chemotherapy.

**Experimental Design:** In mice bearing SF188V+ human glioma xenografts, measurements of temozolomide pharmacokinetic properties and sunitinib pharmacodynamic activities were evaluated, the latter including determinants for vascular normalization, including CD31, collagen IV, and α-SMA.

**Results:** Sunitinib given in a daily dose of either 10 or 40 mg/kg orally over 14 days increased temozolomide tumor distribution, as indicated by the tumor-to-plasma AUC ratio compared with control; however, only the 10 mg/kg group reached statistical significance ($P < 0.05$). From the pharmacodynamic analysis, a "vascular normalization index" incorporating the microvessel density (MVD) and protein expression of α-SMA and collagen IV was proposed as an indication of the number of tumor vessels with relatively good quality, which was found to be significantly correlated with the unbound temozolomide AUC in tumor interstitial fluid ($P = 0.05$). Furthermore, both sunitinib-treated groups maintained the molecular balance between angiopoietins Ang-1 and Ang-2, suggesting a critical role of angiopoietins in vascular normalization.

**Conclusions:** Several important factors relevant to the antiangiogenic agent – induced tumor vascular normalization have been identified and incorporated into a vascular normalization index that may serve to correlate the angiogenic phenotype to the distribution of cytotoxic drugs in solid tumors.

The recognition of angiogenesis as an indispensable requirement for the growth and dissemination of solid tumors has prompted the development of therapeutic strategies to incorporate drugs not only targeted to tumor cells but also to the tumor vasculature, which, as a drug target, is more accessible, genetically stable, and less susceptible to develop drug resistance than tumor cells (1–4).

Many preclinical and clinical studies conducted to examine the antitumor activity of cytotoxic agents and angiogenic inhibitors in combination have shown at least additive, if not synergistic, effects (5–7). The underlying mechanisms for those beneficial effects are not fully understood. Several purported explanations include the direct enhancement of the sensitivity of tumor cells to the cytotoxic therapeutics (8, 9), as well as the improved delivery of therapeutic molecules to solid tumors through vascular normalization and reduced tumor interstitial fluid pressure (IFP; refs. 10–12). However, as antiangiogenic therapies aim to eliminate tumor blood vessels, one would expect that the resultant decreases in tumor MVD might compromise the access of chemotherapeutic agents to the tumor.

Among the variety of antiangiogenic agents being developed, the small molecule kinase inhibitors targeting receptor tyrosine kinases have been the most prolific. Sunitinib is an orally active indolinone-based multitargeted kinase inhibitor with antiangiogenic and antitumor activities attributable to the inhibition of several related tyrosine kinase receptors, including vascular endothelial growth factor receptors (VEGFR1-VEGFR3), platelet-derived growth factor receptors (PDGFRα and PDGFRβ), stem cell factor receptor, and FMS-like tyrosine kinase 3 (13, 14). Both preclinical and clinical studies have shown that sunitinib has a broad spectrum of antitumor activity when used as monotherapy (14–17). Furthermore, the combination of sunitinib with different cytotoxic drugs, including docetaxel, fluorouracil, doxorubicin, and cisplatin, potentiates the antitumor activity of these drugs (15, 18, 19). However, there is no information available regarding the effect of sunitinib on the tumor availability of anticancer drugs.

In this study, the intratumoral availability of temozolomide in the presence of sunitinib was examined in the SF188 human

**Authors' Affiliation:** Department of Pharmaceutical Sciences, School of Pharmacy, Temple University, Philadelphia, Pennsylvania
Received 10/8/07; revised 12/10/07; accepted 12/12/07.
**Grant support:** NIH grants CA72937 and CA85577 (J.M. Gallo).
The costs of publication of this article were defrayed in part by the payment of page charges. This article must therefore be hereby marked *advertisement* in accordance with 18 U.S.C. Section 1734 solely to indicate this fact.
**Requests for reprints:** James M. Gallo, Department of Pharmaceutical Sciences, School of Pharmacy, Temple University, 3307 North Broad Street, Philadelphia, PA 19140. Phone: 215-707-9699; Fax: 215-707-9409; E-mail: jmgallo@temple.edu.

doi:10.1158/1078-0432.CCR-07-4544

glioma xenograft model overexpressing vascular endothelial growth factor (20). Temozolomide is an oral imidazotetrazinone methylating agent with potent activity against recurrent and refractory high-grade glioma and metastatic melanoma (21, 22). Our previous studies showed the apparent paradoxical effect of a methionine aminopeptidase inhibitor, TNP-470 (23), and a selective vascular endothelial growth factor receptor inhibitor, SU5416 (24), on the tumor distribution of temozolomide in subcutaneous and intracerebral glioma xenograft models. Others have also found disparate effects of angiogenesis inhibitors on drug penetration into tumors (25, 26). For example, in the study by Dickson et al. (26), the intratumoral drug penetration of topotecan was significantly increased in mice receiving daily bevacizumab administration on day 3, but was not different from the vehicle control on day 7. However, these investigations, as well as our early studies, did not fully consider many of the factors that could impinge upon drug penetration into tumors. Thus, the objective of the current study was to not only measure the pharmacokinetic characteristics of temozolomide when combined with sunitinib but also to identify molecular determinants that could better delineate the basis for any drug interactions.

## Materials and Methods

***Materials.*** Temozolomide was generously provided by Schering-Plough Research Institute. Sunitinib was supplied by Dr. M.V. Reddy (Fels Institute for Cancer Research, Temple University) and dissolved in 0.1 mol/L citrate buffer (pH 4.7) at a stock concentration of 2 mg/mL. All other chemicals and solvents were obtained from commercial sources.

Male NIH Swiss nude mice (nu/nu, 6-7 weeks old) were purchased from National Cancer Institute. The care and use of animals was approved by the Institutional Animal Care and Use Committee in accordance with NIH guidelines.

A human SF188 glioma cell line that was transfected with the mouse full-length $VEGF_{164}$ cDNA as reported previously (21) and thereby overexpressing vascular endothelial growth factor (V+) was grown in DMEM supplemented with 10% standard fetal bovine serum and maintained in a humidified atmosphere of 5% $CO_2$ in air at 37°C.

***Mouse tumor model and treatment regimens.*** SF188V+ tumor cells ($5 \times 10^6$) suspended in 0.2 mL Matrigel (BD Biosciences) were inoculated s.c. in the dorsal neck region of the nude mice. Tumor growth was monitored twice a week with the volumes calculated as $0.5 \times \text{length} \times \text{width}^2$ (27). At a tumor size of ~500 $mm^3$, nude mice were randomized into three groups: (*a*) the vehicle control group (daily oral administration of 0.1 mol/L citrate buffer at pH 4.7), (*b*) the 10 mg/kg sunitinib group (10 mg/kg sunitinib orally daily for up to 14 days), and (*c*) the 40 mg/kg sunitinib group (40 mg/kg sunitinib orally daily for up to 14 days).

***Measurement of tumor IFP.*** Tumor IFP was measured in both central and peripheral regions of the tumor using the "wick-in-needle" technique as described elsewhere (28) 1 day before the initiation of sunitinib treatment and weekly thereafter.

***Single-dose temozolomide administration and blood and tumor microdialysis sampling.*** Fourteen days after the initiation of vehicle or sunitinib treatment, a subgroup of tumor-bearing mice from each group ($n = 7$ for each) received a single oral dose of temozolomide (20 mg/kg) and underwent pharmacokinetic measurements. A carotid artery catheter was inserted 1 day before temozolomide dosing for blood sampling. Blood samples were taken before, at 2, 5, 15, and 30 minutes, and at 1, 2, 3, 4, 5, and 6 hours after temozolomide administration. Blood drawn was replaced with 20 μL of heparinized saline (10 units/mL) after each collection to avoid volume depletion. Plasma was separated by centrifugation and then stored at -80°C until analyzed for temozolomide. To determine unbound temozolomide concentrations in interstitial fluid (IF), tumor microdialysis was done, as previously described (29). In brief, CMA/20 dialysis probes with a membrane length of 10 mm and a molecular weight cutoff of 20 kDa were inserted into the central region of the tumor and perfused with Ringer's solution at a flow rate of 1 μL/min. Before the administration of temozolomide, individual probe recovery values of temozolomide were determined using the retrodialysis method described previously (29). After a wash-out period of 40 minutes, a single oral dose of 20 mg/kg temozolomide was given, and microdialysis sampling was continued at 20-minute intervals up to 6 hours. Samples were stored at -80°C until analyzed for temozolomide. The percentage of relative recoveries (mean ± SD) of temozolomide from tumor IF were 40.9 ± 7.0, 35.9 ± 8.4, and 36.9 ± 3.4 for the control, 10 mg/kg, and 40 mg/kg sunitinib groups, respectively.

***Quantitative analysis of temozolomide.*** Temozolomide concentrations in plasma and tumor microdialysate were quantitated using a validated high-pressure liquid chromatography method with UV detection as reported previously with minor modifications (24). Standard curves of temozolomide were linear within the ranges of 100 to 50,000 ng/mL ($r^2 = 0.99$) and 20 to 50,000 ng/mL ($r^2 = 0.99$) in plasma and microdialysate, respectively. The low limit of quantification was 100 and 20 ng/mL for temozolomide in plasma and microdialysate, respectively. The mean extraction recovery was 98.4% and 103.1% for plasma and tumor microdialysate, respectively. The intraassay and interassay precisions were all <15%, and the accuracy expressed as the percentage error was within the range of ±15% for both plasma and tumor microdialysate.

***Pharmacokinetic analysis.*** Pharmacokinetic data analyses were done using the software package SAAM II (version 1.2, University of Washington). A hybrid pharmacokinetic model was developed in a sequential manner that consisted of a forcing function describing the plasma concentration-time profile and a one-compartment tumor model characterizing drug disposition in the tumor, as described previously (29). Model fitting used maximum likelihood optimization (30), and goodness-of-fit was assessed by examination of SEs of the estimates and inspection of the Akaike Information Criterion, i.e., the smallest Akaike Information Criterion value was associated with the best-fit model.

Due to the limited number of blood sampling times available in each animal, the absorption of temozolomide after a single oral administration of 20 mg/kg temozolomide was characterized in a separate group of animals. Because the resultant absorption rate constant ($K_a$) values did not vary significantly in the presence and absence of sunitinib, $K_a$ was fixed at the mean value of 17.5 per hour for all three study groups in the hybrid pharmacokinetic model. Variables estimated in the model included the apparent volume of distribution ($V/F$), the elimination rate constant ($K_e$), the intercompartmental rate constants (i.e., $K_{pt}$ and $K_{tp}$) in which all factors that modify transport, such as diffusion or convection, are lumped together, and the area under the plasma or tumor IF concentration-time curve ($AUC_{0\to t,p}$ and $AUC_{0\to t,t}$ for plasma and tumor IF, respectively) from 0 to the last quantifiable time point. The volume of the tumor compartment ($V_t$) was fixed as the actual tumor volume measured in individual animals on the day of pharmacokinetic sampling. Pharmacokinetic variables calculated from these estimates included the systemic oral clearance ($CL_p/F$) and the total areas under the concentration-time curves ($AUC_{0\to\infty}$). The peak plasma concentration ($C_{max}$) and the peak time ($t_{max}$) were obtained by visual inspection of the plasma and tumor IF concentration-time curves.

***Immunohistochemistry.*** The vasculature of the vehicle-treated and sunitinib-treated tumors was evaluated using the immunohistochemical markers for endothelial cells (CD31), blood vessel basement membranes (collagen IV), and mural cells, i.e., pericytes and smooth muscle cells (α-SMA). Cryostat tumor sections were fixed in cold acetone, 1:1 acetone/chloroform, and acetone (5 minutes for each). After a PBS (pH 7.5) wash and incubation with 3% $H_2O_2$ in methanol

for 20 minutes at room temperature to quench endogenous peroxidase, sections were incubated overnight at 4°C with the appropriate dilutions of anti-CD31 (1:400; rat monoclonal, BD PharMingen), anti–collagen IV (1:100; rabbit polyclonal, Millipore Chemicon), or anti–α-SMA (1:100; mouse monoclonal, clone 1A4, Sigma-Aldrich Co.) primary antibodies. This was followed by a 1-hour incubation with biotinylated antirat (for CD31), antirabbit (for collagen IV), or antimouse (for α-SMA) IgG (1:200; Vector Laboratories). The remaining steps were done using the Vectastain Elite ABC kit (Vector Laboratories) for CD31 or the Vectastain Alkaline Phosphatase kit for collagen IV and α-SMA based on the manufacturer's protocols. All sections were counterstained with Gill's No. 3 hematoxylin (Sigma-Aldrich Co.).

***Quantitation of immunostaining and evaluation of vascular normalization.*** Digital images (Leica DC500 camera and DM4000B microscope) were semiquantitated for each marker (i.e., CD31, collagen IV, and α-SMA) in each tumor sample by measuring the pixel area of the positive staining of individual markers in six random areas at 200× magnification using the Image-Pro Plus 5.1 software (Media Cybernetics). The results were presented as the percentage of marker-positive area, which is calculated as marker-positive area × 100 / area of optical field.

Tumor blood vessels, like normal vessels, consist of endothelial cells, mural cells, and their enveloping basement membrane, yet they are structurally and functionally abnormal. This is thought to be in part due to the abnormal proliferation of endothelial cells, defects in the basement membrane, and the alteration in the number of associated pericytes (3, 31, 32). Vascular normalization by antiangiogenic therapy is expected to result in greater coverage of pericytes and a more normal thickness of the basement membrane, thereby improving both the structure and function of tumor vessels. In the present study, we proposed a vascular normalization index (VNI) to assess the normality of tumor vessels related to drug penetration. The VNI was expressed as

$$\mathrm{VNI} = \mathrm{MVD} \times \frac{\mathrm{Density}_{\alpha-\mathrm{SMA}}}{\mathrm{Density}_{\mathrm{CollagenIV}}}$$

where MVD is determined by CD31 immunostaining and expressed as the percentage of CD31-positive area relative to the area of optical field. $\mathrm{Denstiy}_{\alpha\text{-SMA}}$ is the percentage of α-SMA–positive area, and $\mathrm{Density}_{\mathrm{Collagen\ IV}}$ is the percentage of collagen IV–positive area relative to the area of the optical field. The ratio of $\mathrm{Density}_{\alpha\text{-SMA}}$ to $\mathrm{Density}_{\mathrm{Collagen\ IV}}$ represents the extent of the increase in the pericyte coverage and reduction in the thickness of the basement membrane.

***Quantitative real-time PCR assay.*** Isolation of total RNA from tumor tissues and reverse transcription synthesis of cDNA were done as described earlier (29). Real-time PCR was conducted according to the manufacturer's protocol using the predeveloped 20× TaqMan gene expression assay mix (Applied Biosystems) for the following genes: human *HIF-1α* (Hs00936368_m1), murine *Ang-1* (Mm00456503_m1), murine *Ang-2* (Mm00545822_m1), murine *PDGFRβ* (Mm00435546_m1), murine *Col4a1* (Mm00802372_m1), and human *β-actin* (the endogenous control, Hs99999903_m1). Each RNA sample was tested in quadruplicate, and the $C_t$ values were averaged. The relative amounts of the five genes were calculated by means of the $\Delta\Delta C_t$ method as previously described (29).

***Semiquantitative Western blot analysis.*** Tumor homogenates were prepared, and proteins were separated and transferred to nitrocellulose membranes, as previously described (29). Western blotting was probed with 1:400 diluted rabbit polyclonal anti-PDGFRβ (Santa Cruz Biotechnology) and 1:4,000 diluted mouse monoclonal anti–β-actin (Sigma-Aldrich) primary antibodies and subsequently treated with 1:20,000 diluted IRDye 680–conjugated goat anti-rabbit and IRDye 800CW–conjugated goat anti-mouse secondary antibodies (LI-COR Biosciences). Proteins were visualized and quantitated with the Odyssey IR imaging system (LI-COR Biosciences).

***Statistical analysis.*** Number Cruncher Statistical Systems 2004 was used for statistical evaluation of data. All data are presented as the mean ± SD. Comparison of means between two related samples and between two independent groups was made using paired and two-sample *t* test, respectively. In case of multiple comparisons, Kruskal-Wallis one-way ANOVA on ranks followed by the post-hoc Kruskal-Wallis multiple comparison *z* value test was used. Pearson correlations were used to describe relations between two variables. A two-sided *P* value of <0.05 was considered statistically significant.

## Results

***Effect of sunitinib on the disposition of temozolomide in plasma and tumor.*** The pharmacokinetic study of single-dose temozolomide was conducted in tumor-bearing mice using serial blood sampling in conjunction with microdialysis to assess temozolomide concentrations in plasma and tumor IF, respectively. The one compartment open model with first-order absorption and elimination was found adequate for the temozolomide plasma concentration-time data in tumor-bearing mice receiving either vehicle, 10 mg/kg sunitinib, or 40 mg/kg sunitinib for 14 days. Similar $C_{max}$ and $t_{max}$ values for temozolomide found between the control and sunitinib treatment groups indicate no apparent effect of sunitinib on the absorption of temozolomide (Table 1). The systemic exposure of temozolomide was analogous in the individual groups of animals with mean (±SD) $AUC_{0\to\infty}$ values of 25.9 ± 3.1, 26.3 ± 4.0, and 25.4 ± 6.5 μg h/mL for the control, 10 mg/kg, and 40 mg/kg sunitinib groups, respectively, suggesting that there is no significant difference in the systemic disposition kinetics of temozolomide among the three experimental groups (Fig. 1A; Table 1).

Unlike the systemic pharmacokinetic properties of temozolomide, local alterations in temozolomide tumor concentrations were found in the presence of sunitinib (Fig. 1B). The compartmental model applied to temozolomide concentrations in both plasma and tumor IF showed close agreement between predicted and observed values (Fig. 1C-E). As shown in Table 1, the 14-day treatment of 10 mg/kg sunitinib resulted in significantly ($P < 0.05$) elevated temozolomide tumor IF $C_{max}$ (by 49%) compared with the control group, whereas the time to reach the tumor $C_{max}$ (i.e., $t_{max}$) were similar. Also the $AUC_{0\to\infty}$ of unbound temozolomide in the tumor IF was increased by 42% in the 10 mg/kg sunitinib group and 16% in the 40 mg/kg sunitinib group compared with the control group, although these differences in $AUC_{0\to\infty}$ did not reach statistical significance ($P > 0.05$). Nonetheless, the more tell-tale variable of changes in tissue distribution, the mean $AUC_{tumor}/AUC_{plasma}$ ratio, was increased by 42% and 21% in the 10 and 40 mg/kg sunitinib groups, respectively, compared with controls; however, only the difference in the 10 mg/kg group reached statistical significance ($P < 0.05$; Table 1). Therefore, temozolomide penetration into tumor was enhanced due to sunitinib compared with control.

***Assessment of tumor vasculature and its possible association with temozolomide distribution in tumor.*** To examine whether intratumoral temozolomide distribution would be associated with tumor vascularity, tumor samples collected after the pharmacokinetic study were subject to immunohistochemical analysis. MVD and collagen IV density in the 10 mg/kg sunitinib group were moderately decreased by 35% and 26%, respectively, relative to those of the control group ($P > 0.05$ for both), whereas the decreases in the MVD (by 77%) and collagen IV density (by 52%) in the 40 mg/kg sunitinib group

**Table 1.** Pharmacokinetic variables (mean ± SD) of temozolomide in plasma and subcutaneous tumor IF in SF188V+ tumor-bearing mice after oral administration of temozolomide (20 mg/kg) in the absence and presence of sunitinib

| Variables | Control | Sunitinib (10 mg/kg/d) | Sunitinib (40 mg/kg/d) |
|---|---|---|---|
| *n* | 7 | 7 | 7 |
| Plasma | | | |
| $C_{max}$ (μg/mL) | 21.2 ± 5.2 | 19.5 ± 2.1 | 19.2 ± 6.7 |
| $t_{max}$ (h) | 0.083 ± 0.000 | 0.15 ± 0.09 | 0.11 ± 0.06 |
| $AUC_{0\to\infty}$ (μg·h/mL) | 25.9 ± 3.1 | 26.3 ± 4.0 | 25.4 ± 6.5 |
| $t_{1/2}$ (h) | 0.784 ± 0.314 | 0.793 ± 0.165 | 0.725 ± 0.395 |
| $K_e$ ($h^{-1}$) | 1.06 ± 0.54 | 0.91 ± 0.23 | 1.20 ± 0.60 |
| *V/F* (L/kg) | 0.881 ± 0.319 | 0.881 ± 0.156 | 0.841 ± 0.345 |
| $CL_p/F$ (L/h/kg) | 0.797 ± 0.097 | 0.785 ± 0.129 | 0.864 ± 0.249 |
| Tumor IF | | | |
| $C_{max}$ (μg/mL) | 10.6 ± 3.6 | 15.8 ± 4.4* | 12.7 ± 2.7 |
| $t_{max}$ (h) | 0.690 ± 0.178 | 0.776 ± 0.098 | 0.833 ± 0.000 |
| $AUC_{0\to\infty}$ (μg·h/mL) | 20.4 ± 6.7 | 28.9 ± 8.6 | 23.7 ± 8.3 |
| $AUC_{0\to\infty}$ ratio | | | |
| $AUC_{tumor}/AUC_{plasma}$ | 0.780 ± 0.234 | 1.104 ± 0.289 * | 0.946 ± 0.232 |
| Intercompartmental rate constant | | | |
| $K_{pt}$ ($h^{-1}$) | 5.06 ± 4.16 | 3.97 ± 1.69 | 2.00 ± 1.14 † |
| $K_{tp}$ ($h^{-1}$) | 3.98 ± 2.83 | 2.97 ± 0.98 | 2.63 ± 1.05 |

Abbreviations: $C_{max}$, peak concentration; $t_{max}$, time to reach peak concentration; $AUC_{0\to\infty}$, total area under the concentration-time curve; $t_{1/2}$, half life; $K_e$, elimination rate constant; *V/F*, apparent volume of distribution; $CL_p/F$, systemic oral clearance; $K_{pt}$ and $K_{tp}$, intercompartmental rate constants.
*$P < 0.05$ compared with the vehicle control group using equal variance *t* test.
†$P < 0.05$ compared with the 10 mg/kg sunitinib treatment group using equal variance *t* test.

were highly significant compared with the control group ($P < 0.01$ for both; Fig. 2A). No significant differences in the α-SMA density were observed among the control and two sunitinib groups (Fig. 2A). In animals used in the pharmacokinetic analyses, the VNI values had the rank order of 10 mg/kg sunitinib (1.5%) > vehicle control (1.2%) > 40 mg/kg sunitinib (1.1%); however, the differences were not statistically different. When the same data from all treatment groups were pooled, statistically significant correlations were found between the α-SMA density and temozolomide tumor IF AUC ($P = 0.016$; Fig. 2B) and between the VNI value and temozolomide tumor IF AUC ($P = 0.050$; Fig. 2C).

***Tumor response to sunitinib treatment.*** The antitumor and antiangiogenic effect of sunitinib was scrutinized in a second cohort of animals to gain a better understanding as to what factors may contribute to the tumor penetration of cytotoxic drug coadministered with antiangiogenic therapy. Sunitinib treatment at doses of 10 and 40 mg/kg/day was found to be well tolerated with no noticeable body weight loss or overt toxicity compared with the vehicle group (data not shown). Tumor growth was significantly inhibited by 29% and 50% in 10 and 40 mg/kg sunitinib groups, respectively, compared with the control group ($P < 0.01$; Fig. 3A). Sunitinib treatment at 40 mg/kg significantly reduced the tumor IFP by ~40% relative to that of the control group ($P < 0.01$), whereas the decrease in the tumor IFP in the 10 mg/kg sunitinib group (by 21%) was not statistically significant (Fig. 3B).

***Mechanisms underlying the antivascular effect of sunitinib in SF188V+ tumors—histologic analyses.*** We wanted to examine the antivascular effect of sunitinib in animals that did not participate in the pharmacokinetic study and, thus, eliminate any potential deleterious effects of microdialysis probes on tumor histology. Tumor samples were harvested from five animals per group per time point at two time points (7 and 14 days) after the initiation of sunitinib treatment with half the tumor used for histologic examination and the other half for molecular analyses. In line with the earlier results, microscopic examination of tumor sections stained for CD31, collagen IV, and α-SMA clearly showed that sunitinib reduced tumor MVD and collagen IV density in a dose-dependent manner on both days 7 and 14 (Fig. 4A). In contrast and similar to pharmacokinetic study results, the α-SMA density was not significantly changed in both 10 and 40 mg/kg sunitinib groups over the 2-week treatment period ($P > 0.05$ for all; Fig. 4B). Additionally, on day 7, the mean VNI values were found to decrease in the order of 10 mg/kg sunitinib (2.2%) > 40 mg/kg sunitinib (2.1%) > vehicle control (1.1%); whereas on day 14, the mean VNI values were decreased in all three groups with the rank order similar to that observed in the tumor samples of the pharmacokinetic study, i.e., 10 mg/kg sunitinib (1.7%) > vehicle control (1.2%) ≈ 40 mg/kg sunitinib (1.2%; Fig. 4B), yet the differences between the treatment groups were also not significantly different ($P > 0.05$).

***Mechanisms underlying the stabilization effect of sunitinib on tumor vasculature in SF188V+ tumors—real-time PCR and Western blot analyses.*** In addition to the histologic analyses, we also examined molecular events possibly associated with the antivascular effect of sunitinib with an emphasis on determining how antiangiogenic therapy with sunitinib could lead to vascular normalization. Angiopoietins are known to play an important role in the development of the immature vasculature. Ang-1 is critically involved in the maturation and maintenance of the vascular plexus (33), whereas Ang-2 promotes the remodeling of the mature vasculature and vascular sprouting in the presence of vascular endothelial growth factor (34, 35). The results of the quantitative real-time

PCR showed that sunitinib treatment had no effect on the *Ang-1* mRNA expression level in SF188V+ xenografts irrespective of dose levels ($P > 0.05$), but decreased the *Ang-2* mRNA expression level on both days 7 and 14 in a dose-dependent manner, although the statistically significant reduction relative to the control group was only found in the 40 mg/kg sunitinib group ($P < 0.05$; Fig. 5A and B). As a result, the *Ang-1*/*Ang-2* gene expression ratio, which indicates the instability of the vasculature when declining (36, 37), tended to be increased in both sunitinib treatment groups, although the increase was not statistically significant compared with the control group ($P > 0.05$; Fig. 5A and B).

The expression level of *Col4a* gene, which is one of the six distinct genes encoding the triple helical α-chains of type IV collagen, was reduced by 11% and 62% by the 10 and 40 mg/kg sunitinib treatment, respectively, and the reduction was found statistically significant in the 40 mg/kg sunitinib group ($P < 0.05$; Fig. 5A and B). In line with the immunohistochemical analysis results, this result suggests a dose-dependent inhibitory effect of sunitinib on collagen IV expression on the mRNA level.

Reduction in tumor blood vessel density caused by angiogenic inhibition may exacerbate hypoxia in tumor. On this basis, we evaluated the expression of *HIF-1α* mRNA as an indirect index of oxygenation of the tumor. Sunitinib treatment did not up-regulate *HIF-1α* mRNA expression levels in the tumor; rather, the expression level of *HIF-1α* mRNA was moderately reduced by 18% in the 10 mg/kg sunitinib group, presumably due to the increased delivery of oxygen resulting from the improved efficiency of the tumor vasculature (Fig. 5A and B).

Sunitinib is the inhibitor of multiple receptor tyrosine kinases, including PDGFRβ. As expected, sunitinib treatment decreased both mRNA and protein expression levels of PDGFRβ in a dose-dependent manner, but to varying degrees (Fig. 5A-D). The less percentage inhibition of PDGFRβ protein expression compared with that of *PDGFRβ* mRNA expression may be due to the limited specificity of Western blot technique in distinguishing between the tumor and blood vessel origins of PDGFRβ. The expression levels of Ang-1, Ang-2, and HIF-1α proteins were not detectable by Western blotting.

## Discussion

As new antiangiogenic agents continue to emerge in cancer therapy, a prominent challenge is how to integrate these novel agents into effective treatment paradigms. It is particularly challenging to evaluate potential combination therapies with angiogenesis inhibitors because of the lack of well-established preclinical models, and the associated difficulties of defining optimal biological doses and elucidating adequate surrogate markers for drug response. In our previous studies, differential effects of antiangiogenic agents were observed on tumor concentrations of temozolomide, demonstrating the importance of assessing the role of all variables that may affect the

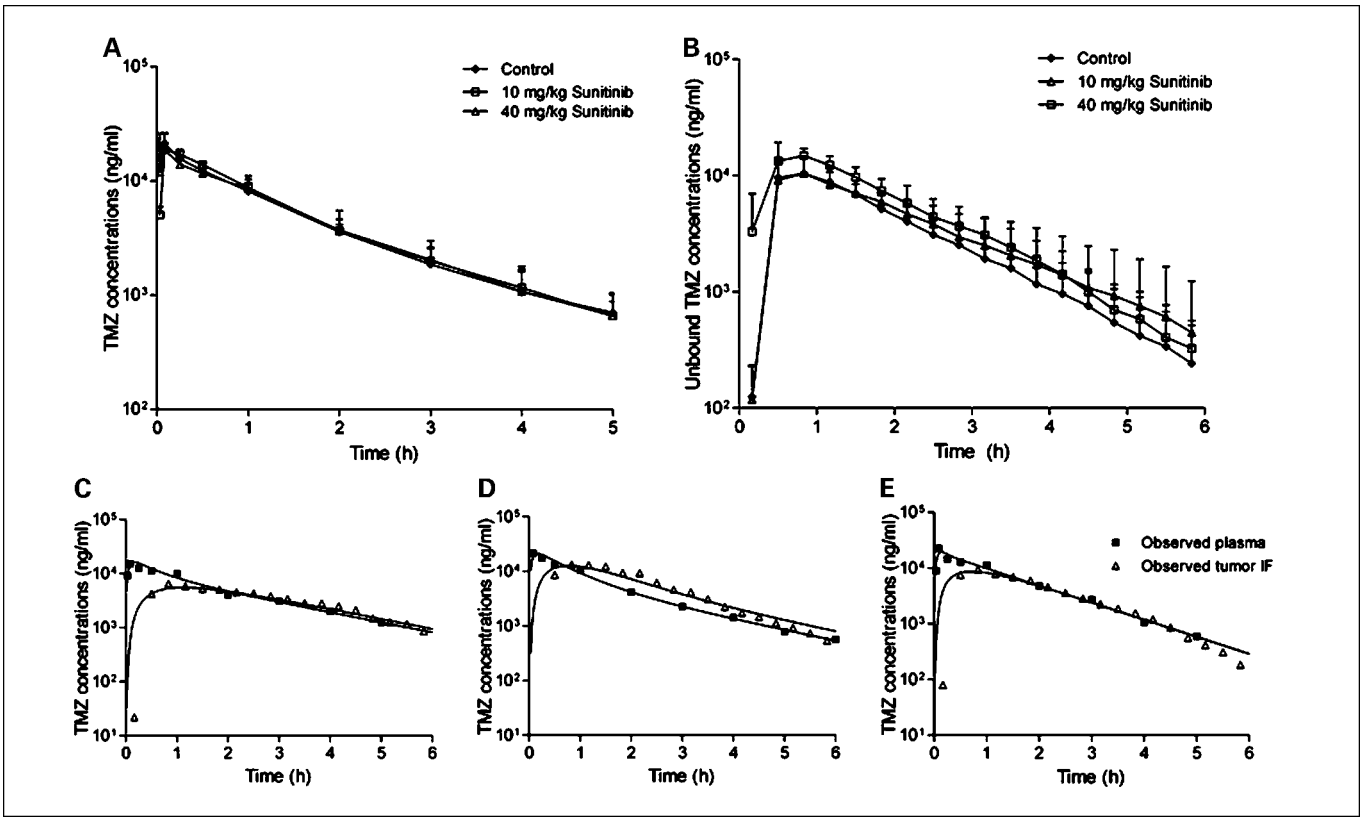


**Fig. 1.** Time courses of plasma (*A*) and tumor IF (*B*) concentrations (mean ± SD) for temozolomide after the oral administration of single-dose temozolomide (20 mg/kg) to tumor-bearing mice treated with the vehicle (*closed rhombi*), 10 mg/kg/d sunitinib (*open squares*), or 40 mg/kg/d sunitinib (*open triangles*) for 14 consecutive days (seven animals per group). Representative model-predicted (—) and observed temozolomide plasma (*closed squares*) and tumor IF (*open triangles*) concentrations in three SF188V+ tumor-bearing mice receiving single-dose 20 mg/kg temozolomide after 14-d treatment of the vehicle (*C*), 10 mg/kg/d sunitinib (*D*), and 40 mg/kg/d sunitinib (*E*), respectively. Bars, SD.

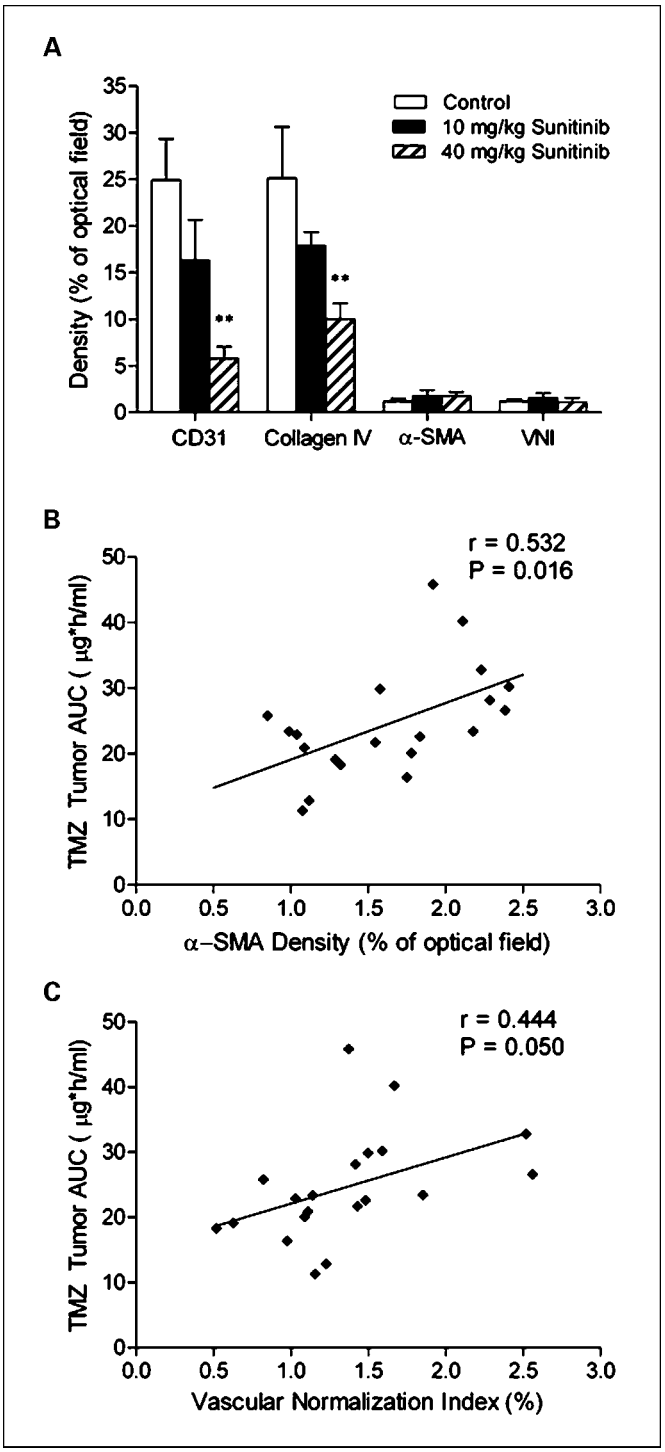


**Fig. 2.** *A,* immunohistochemical analyses of MVD, collagen IV density, and α-SMA density in the SF188V+ tumor sections obtained from the control, 10 mg/kg sunitinib – treated, and 40 mg/kg sunitinib – treated tumor-bearing mice after the single-dose temozolomide pharmacokinetic study as described in Materials and Methods. MVD and collagen IV density relative to the control tumors were significantly decreased in the 40 mg/kg sunitinib – treated tumors ($P < 0.01$, Kruskal-Wallis one-way ANOVA on ranks followed by the post-hoc Kruskal-Wallis multiple comparison *z* value test). Columns, mean; bars, SD. *B,* the unbound temozolomide AUC in tumor IF in relation to the α-SMA density obtained by immunostaining for α-SMA, the marker for vascular mural cells, in the SF188V+ tumor sections ($P = 0.016$, $n = 20$, Pearson's Correlation test). *C,* the unbound temozolomide AUC in tumor IF in relation to the VNI value calculated as MVD × ($Density_{\alpha\text{-SMA}}$ / $Density_{Collagen\ VI}$; $P = 0.05$, $n = 20$, Pearson's Correlation test). *r,* Pearson's correlation coefficient.

delivery of cytotoxic drugs to tumors (23, 24). Towards this end, the present study analyzed numerous biological and molecular determinants of angiogenesis in the context of combination sunitinib and temozolomide treatments.

The findings from this study indicated that the extended treatment with sunitinib at either 10 or 40 mg/kg/day did not affect the systemic pharmacokinetic properties of temozolomide in tumor-bearing mice, suggesting that a direct pharmacokinetic interaction between temozolomide and sunitinib is unlikely. However, the extent of tumor exposure to temozolomide, as indicated by the tumor-to-plasma temozolomide AUC ratio, was increased after a 14-day treatment period of sunitinib. Notably, the effect at the 10 mg/kg dose was statistically different from control (Table 1). Because temozolomide is thought not to undergo any active membrane transport process and the involvement of active transport in

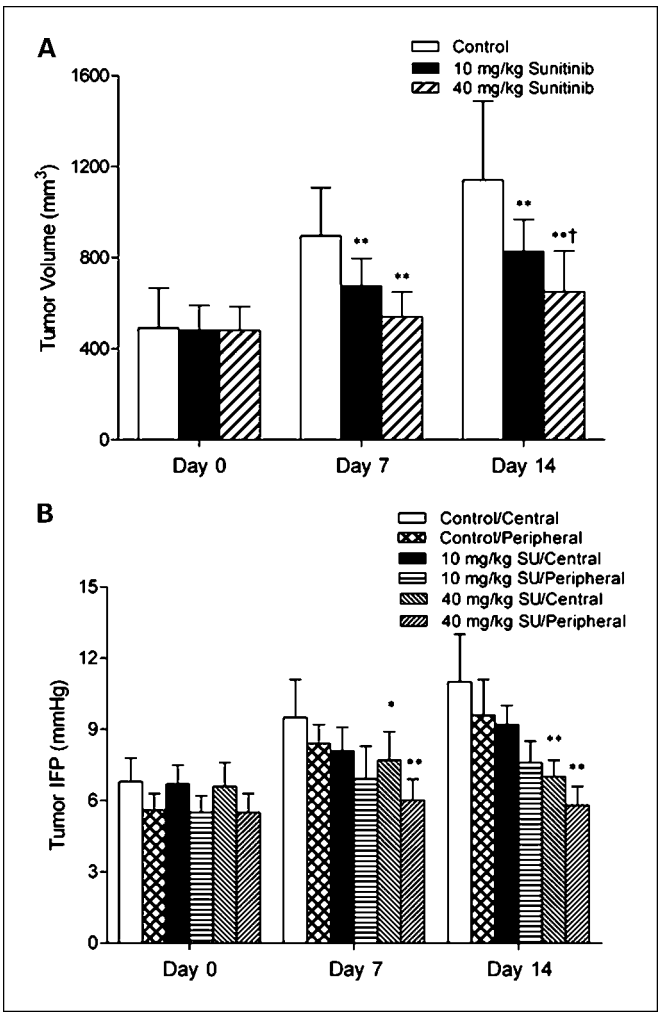


**Fig. 3.** Antitumor activity of sunitinib in mice bearing SF188V+ human glioma xenografts. Nude mice bearing established SF188V+ ( ~ 500 $mm^3$) xenografts were randomized into three groups receiving daily oral administration of vehicle, 10 mg/kg sunitinib, or 40 mg/kg sunitinib for up to 14 d. *A,* the effect of sunitinib on tumor growth ($n = 13$-25). **, $P < 0.01$ compared with the control group. †, $P < 0.01$, compared with the 10 mg/kg sunitinib group. *B,* the effect of sunitinib on tumor interstitial fluid pressure ($n = 5$-10). **, $P < 0.01$ compared with the corresponding region of the tumor in the control group. Statistical significance was assessed by Kruskal-Wallis one-way ANOVA on ranks followed by the post-hoc Kruskal-Wallis multiple comparison *z* value test. Columns, mean; bars, SD.

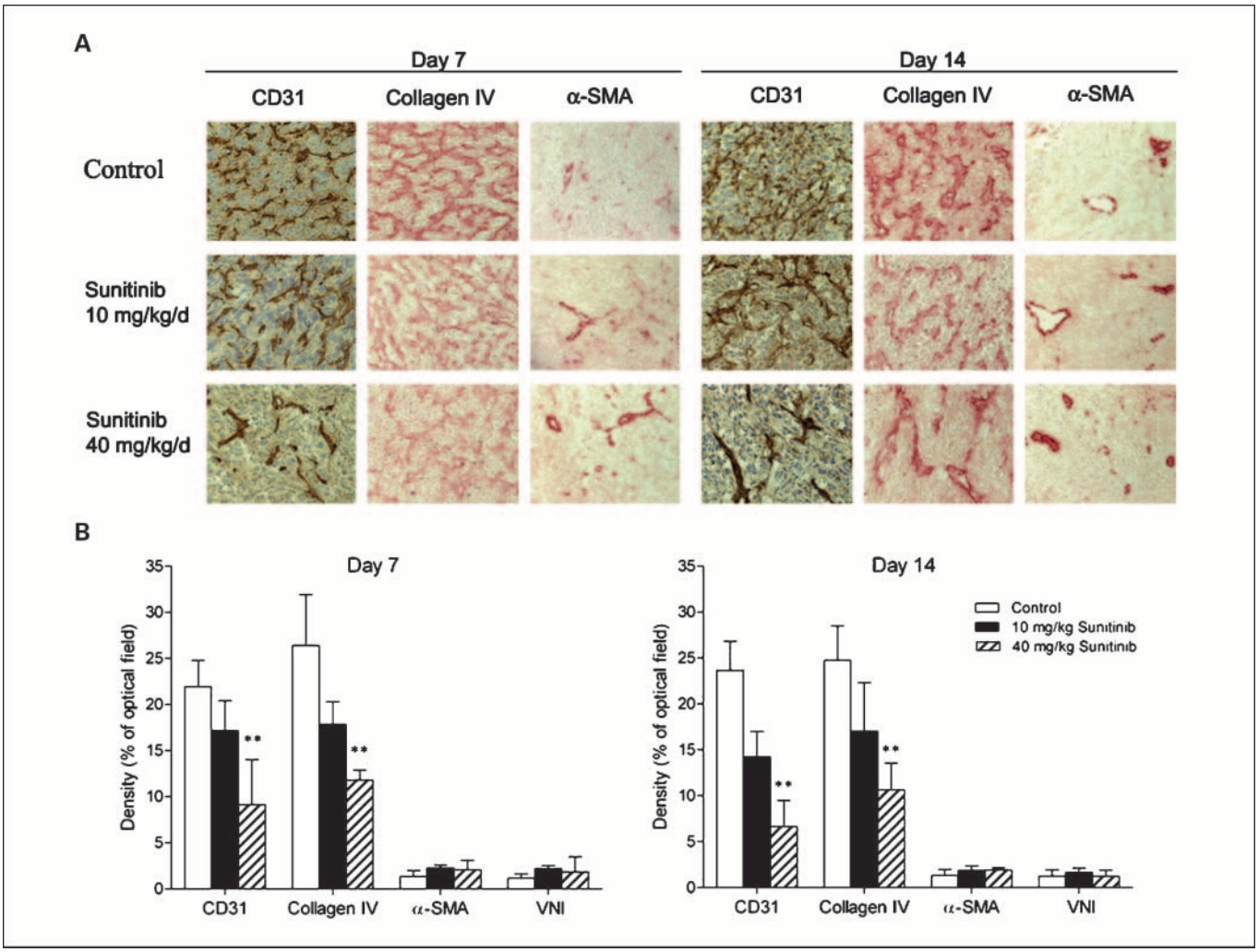


**Fig. 4.** Immunohistologic evaluation of the effect of sunitinib on the intratumoral vasculature within established SF188V+ xenografts. Tumor-bearing mice were sacrificed on days 7 and 14 after the start of the daily administration of either vehicle or sunitinib (five animals per time point per group), and the subcutaneous tumors were excised and processed as described in Materials and Methods. *A,* representative examples for the detection of CD31, collagen IV, and α-SMA in tumor sections from the control and two sunitinib treatment groups. Original magnification, 200× for CD31 and type IV collagen and 100× for smooth muscle actin; *B,* quantitative comparison of CD31-positive, collagen IV – positive, and α-SMA – positive areas of the tumor sections (five to seven regions per section analyzed) from the three groups of animals at two different time points. Image-Pro Plus 5.1 software was used to quantify the immunohistologic results. Representative sections and the quantitative analysis results show a significant decrease in tumor MVD (CD31) and blood vessel basement membrane density (collagen IV) in the 40 mg/kg sunitinib group relative to those in the control group; **, $P < 0.01$. Columns, mean; bars, SD.

the tissue distribution of sunitinib has not been documented, it seemed unlikely that changes in the tumor distribution of temozolomide could be attributed to the direct modulation of membrane transport by sunitinib. Therefore, the sunitinib-induced enhancement in tumor distribution of temozolomide is attributed to pharmacodynamic-mediated changes on vascular normalization and stability and reduction in IFP.

Unlike the normal vasculature, tumor neovasculature is characterized by a tortuous arrangement of endothelial cells, thickened basement membrane, and inadequate pericyte coverage (31, 32). The histologic analysis of the tumor samples obtained from the pharmacokinetic study showed that sunitinib reduced tumor MVD and collagen IV density in a dose-dependent fashion but had no effect on the α-SMA density (Fig. 2A). These findings suggest that sunitinib selectively prunes the most immature newly formed microvessels, reduces basement membrane thickness, and spares the relatively efficient vessels covered by mural cells. However, when the data were pooled irrespective of treatment group, temozolomide tumor uptake was found not to correlate significantly with either tumor MVD or collagen IV density but with the α-SMA density (Fig. 2B). This intriguing observation implicates that the extent of temozolomide tumor distribution may be associated with the number of functioning and partially functioning vessels in the tumor. As the quality of tumor vessels is associated with the basement membrane presence and mural cell coverage, we proposed a VNI as an indication of the number of tumor vessels with relatively good quality, which is expressed as the MVD adjusted by the ratio of the α-SMA density (as an indication of mural cell coverage) to the collagen IV density (as an indication of basement membrane thickness). Those tumor vessels possessing a quality akin to normal capillaries were found more permissive to temozolomide penetration as a significant correlation was found between the VNI value and temozolomide tumor AUC (Fig. 2B). This relationship was based on pooled data from all treatment

groups and indicated the delineation of effects on drug accumulation cannot precisely be segregated by dose level. It is noteworthy that the mean VNI value in the 40 mg/kg sunitinib group on day 14 was decreased by 43% compared with that on day 7 (Fig. 4B), suggesting that continuous sunitinib treatment beyond a normalization window may further destroy the pericyte-enwrapped vessels, leading to compromised drug distribution in the tumor. For the 10 mg/kg sunitinib group, the comparative reduction in the day 7 to day 14 VNI was just 18%, which suggests a vascular normalization window may depend on both the dose and duration of treatment. In this case, optimal treatment regimens of antiangiogenic agents should consider both the duration and dose to facilitate drug penetration into tumors and pharmacodynamic indices, such as the VNI, may provide the quantitative criteria to select the most efficacious regimens.

It is believed that in the presence of a normal vasculature temozolomide crosses membranes by diffusion; however, in tumors, convective transport is influenced by changes in IFP. In this study, the tumor IFP decreased in the sunitinib treatment groups and may have led to protein-bound and unbound temozolomide to extravasate from tumor vessels resulting in higher temozolomide concentrations in tumor IF compared with those attained by diffusional transport alone (38, 39). In light of a recent study demonstrating that an antiangiogenic agent caused a minor increase in the hydrostatic pressure gradient sufficient to increase the transvascular convection of a macromolecule (40), our finding implicates that measurement of both hydrostatic pressure and IFP will be needed to fully evaluate convection-mediated drug transport. It may be found that incorporation of these factors with the VNI will better elucidate the relationship between drug penetration into tumor and the effect of antiangiogenic agent on tumor vasculature.

Several important factors involved in the control of the structure and function of tumor vessels were examined on the level of gene expression. Ang-1 and Ang-2 are among the most important growth factors responsible for the maturation, maintenance, and remodeling of the tumor vascular network. Although the regulatory effect of Ang-1 and Ang-2 on tumor angiogenesis remains controversial, a considerable body of evidence has shown that, in most malignancies, Ang-2 expression is up-regulated to a greater extent compared with Ang-1, leading to a shift in the molecular balance between Ang-1/Ang-2 in favor of Ang-2 (36, 37). Therefore, the ratio

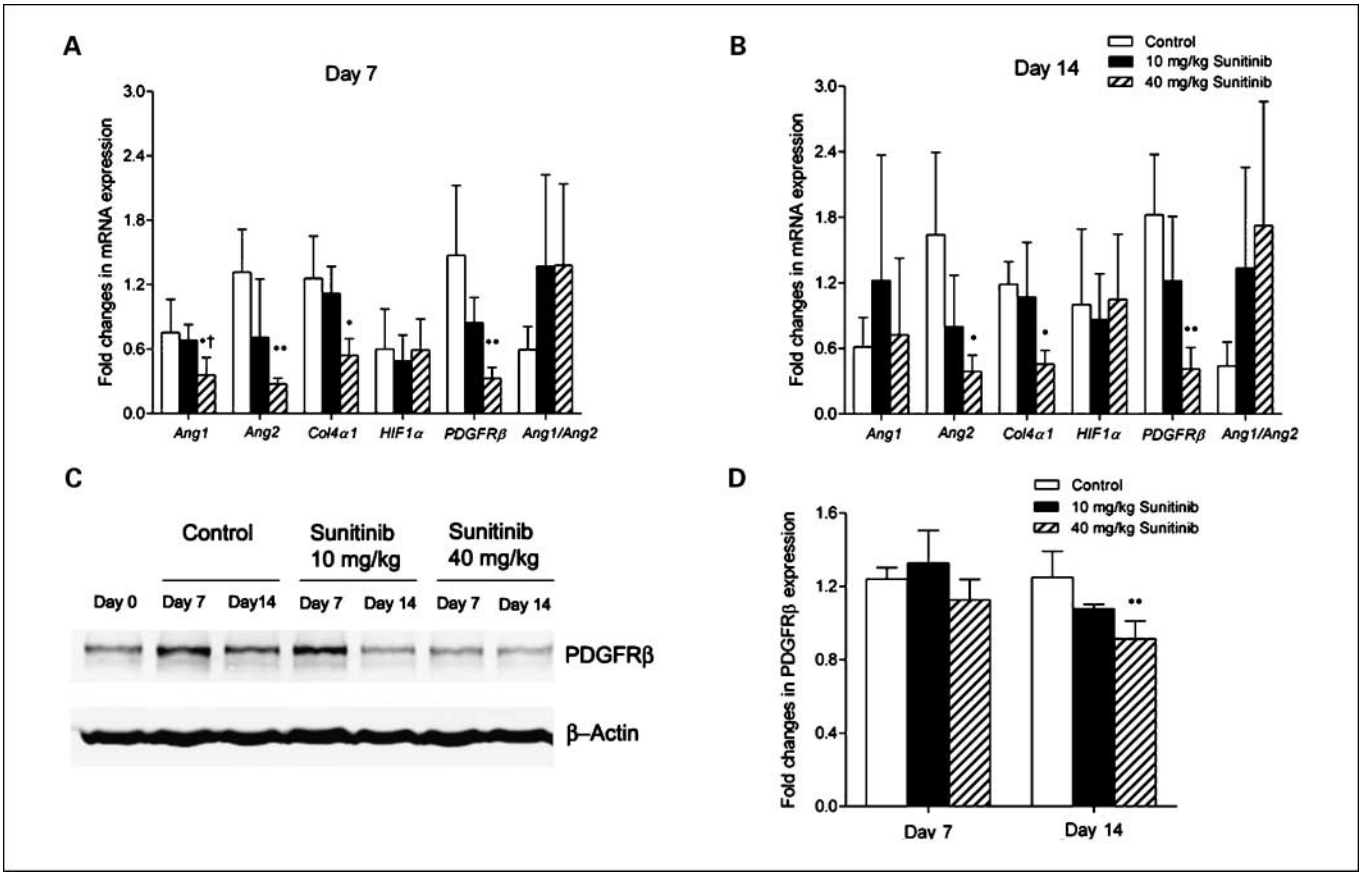


**Fig. 5.** Sunitinib increases the expression levels of certain proangiogenic factors involved in tumor vessel maturation and remodeling and basement membrane synthesis in SF188V+ xenografts in a dose-dependent manner. Tumors were dissected from the vehicle-treated (*open columns*), 10 mg/kg/d (*solid columns*), and 40 mg/kg/d (*hatched columns*) sunitinib-treated animals on day 7 and day 14 after the initiation of the treatment (five animals per time point per group). Relative quantification of the expression levels of murine *Ang-1*, murine *Ang-2*, murine *Col4al*, human *HIF-1α*, and murine *PDGFRβ* mRNA on day 7 (*A*) and day 14 (*B*) was done using the quantitative real-time PCR. The *Ang-1*/*Ang-2* ratio was calculated for individual animals. Western blot analysis as shown in the representative blots (*C*) showed difference among the experimental groups. *D,* densitometric analysis of the immunoblots using the LI-COR Odyssey IR imaging system showed that the expression levels of PDGFRβ protein in tumor was decreased by 14% and 27% in the 10 and 40 mg/kg sunitinib, respectively. Equal loading of protein was confirmed by β-actin. The results are presented relative to the values of the day 0 tumor sample, which is given a value of 1.0. *, $P < 0.05$ and **, $P < 0.01$ compared with the control group; †, $P < 0.05$ compared with the 10 mg/kg sunitinib group. Columns, mean ($n = 5$); bars, SD.

of Ang1/Ang-2 is thought to reflect the degree of active angiogenesis in tumors with reduced ratios indicative of vascular instability. In this study, a dose-dependent down-regulation of *Ang-2* mRNA expression relative to the control tumors was observed in the sunitinib-treated tumors, whereas the mRNA expression levels of *Ang-1* was changed randomly among the three experimental groups. The possible reason is that the main producer of Ang-2 is endothelial cells (41, 42), which is the target of sunitinib treatment, whereas Ang-1 is produced predominantly by vascular mural cells (43, 44), which seemed not to respond to sunitinib in this study. As a result, the *Ang-1/Ang-2* ratio in the two sunitinib treatment groups seemed to be higher than that in the control group, suggesting that continuous sunitinib treatment countered the aberrant vascularization resulting from the imbalance of Ang-1 and Ang-2 in the control group.

In contrast to some early studies demonstrating that the basement membrane of tumor vessels is incomplete or absent, the results from the current study support the notion that basement membrane covers most tumor vessels but may have profound structural abnormalities (31). Our observation of the similar MVD and collagen IV density in tumor sections might be the indirect evidence of the colocalization of endothelial cells and basement membrane in the tumor. In keeping with the histologic analysis observations, the real-time PCR results revealed a dose-dependent reduction in the mRNA expression levels of *Col4a1* in tumor attributable to sunitinib. However, based on the data of the current study, we were unable to evaluate the effect of sunitinib on the abnormality of the vascular basement membrane in the tumor, such as the variable thickness, loose association with endothelial cells and pericytes, and multiple redundant layers. A further confocal microscopic study may be needed to provide this information.

In summary, an increase in the tumor exposure to temozolomide relative to the control mice was found in those treated with sunitinib for 14 days, with the effect greater at the 10 mg/kg dose compared with the 40 mg/kg dose. This suggested a dose-dependent action of sunitinib on tumor penetration that may further be influenced by time-dependent changes of sunitinib in VNI (VNI values were greater on day 7 than day 14; Fig. 4B). The possibility of such combined dose-dependent and time-dependent antiangiogenic effects warrants further evaluation of its relationship to a window of vascular normalization that could better dictate how to combine antiangiogenic and cytotoxic drug therapies. Overall, the findings support a pharmacodynamic basis for positive action of sunitinib on tumor disposition of temozolomide.

## References


1. Folkman J. Tumor angiogenesis: therapeutic implications. N Engl J Med 1971;285:1182–6.
2. Liotta LA, Steeg PS, Stetler-Stevenson WG. Cancer metastasis and angiogenesis: an imbalance of positive and negative regulation. Cell 1991;64:327–36.
3. Hanahan D, Folkman J. Patterns and emerging mechanisms of the angiogenic switch during tumorigenesis. Cell 1996;86:353–64.
4. Kerbel RS. Inhibition of tumor angiogenesis as a strategy to circumvent acquired resistance to anticancer therapeutic agents. Bioessays 1991;13:31–6.
5. Herbst RS, Madden TL, Tran HT, et al. Safety and pharmacokinetic effects of TNP-470, an angiogenesis inhibitor, combined with paclitaxel in patients with solid tumors: evidence for activity in non-small cell lung cancer. J Clin Oncol 2002;20:4440–7.
6. Gerber HP, Ferrara N. Pharmacology and pharmacodynamics of bevacizumab as monotherapy or in combination with cytotoxic therapy in preclinical studies. Cancer Res 2005;65:671–80.
7. Inoue S, Hartman A, Branch CD, et al. mda-7 in combination with bevacizumab treatment produces a synergistic and complete inhibitory effect on lung tumor xenograft. Mol Ther 2007;15:287–94.
8. Jung YD, Mansfield PF, Akagi M, et al. Effects of combination anti-vascular endothelial growth factor receptor and anti-epidermal growth factor receptor therapies on the growth of gastric cancer in a nude mouse model. Eur J Cancer 2002;38:1133–40.
9. Muramaki M, Miyake H, Hara I, Kamidono S. Synergistic inhibition of tumor growth and metastasis by combined treatment with TNP-470 and docetaxel in a human prostate cancer PC-3 model. Int J Oncol 2005;26:623–8.
10. Jain RK. Delivery of novel therapeutic agents in tumors: physiological barriers and strategies. J Natl Cancer Inst 1989;81:570–6.
11. Jain RK. Normalizing tumor vasculature with anti-angiogenic therapy: a new paradigm for combination therapy. Nat Med 2001;7:987–9.
12. Jain RK. Normalization of tumor vasculature: an emerging concept in antiangiogenic therapy. Science 2005;307:58–62.
13. Sun L, Liang C, Shirazian S, et al. Discovery of 5-[5-fluoro-2-oxo-1,2- dihydroindol-(3Z)-ylidenemethyl]-2,4- dimethyl-1H-pyrrole-3-carboxylic acid (2-diethylaminoethyl)amide, a novel tyrosine kinase inhibitor targeting vascular endothelial and platelet-derived growth factor receptor tyrosine kinase. J Med Chem 2003;46:1116–9.
14. Mendel DB, Laird AD, Xin X, et al. *In vivo* antitumor activity of SU11248, a novel tyrosine kinase inhibitor targeting vascular endothelial growth factor and platelet-derived growth factor receptors: determination of a pharmacokinetic/pharmacodynamic relationship. Clin Cancer Res 2003;9:327–37.
15. Abrams TJ, Lee LB, Murray LJ, Pryer NK, Cherrington JM. SU11248 inhibits KIT and platelet-derived growth factor receptor β in preclinical models of human small cell lung cancer. Mol Cancer Ther 2003;2:471–8.
16. O'Farrell AM, Abrams TJ, Yuen HA, et al. SU11248 is a novel FLT3 tyrosine kinase inhibitor with potent activity *in vitro* and *in vivo*. Blood 2003;101:3597–605.
17. Chow LQ, Eckhardt SG. Sunitinib: from rational design to clinical efficacy. J Clin Oncol 2007;13:1367–73.
18. Abrams TJ, Murray LJ, Pesenti E, et al. Preclinical evaluation of the tyrosine kinase inhibitor SU11248 as a single agent and in combination with "standard of care" therapeutic agents for the treatment of breast cancer. Mol Cancer Ther 2003;2:1011–21.
19. Guerin O, Formento P, Lo Nigro C, et al. Supra-additive antitumor effect of sunitinib malate (SU11248, Sutent(R)) combined with docetaxel. A new therapeutic perspective in hormone refractory prostate cancer. J Cancer Res Clin Oncol 2008;134:51–7.
20. Ma J, Fei ZL, Klein-Szanto A, Gallo JM. Modulation of angiogenesis by human glioma xenograft models that differentially express vascular endothelial growth factor. Clin Exp Metastasis 1998;16:559–68.
21. Cohen MH, Johnson JR, Middleton MR. Temozolomide for advanced, metastatic melanoma. J Clin Oncol 2000;18:2185.
22. Dehdashti AR, Hegi ME, Regli L, Pica A, Stupp R. New trends in the medical management of glioblastoma multiforme: the role of temozolomide chemotherapy. Neurosurg Focus 2006;20:E6.
23. Ma J, Pulfer S, Li S, Chu J, Reed K, Gallo JM. Pharmacodynamic-mediated reduction of temozolomide tumor concentrations by the angiogenesis inhibitor TNP-470. Cancer Res 2001;61:5491–8.
24. Ma J, Li S, Reed K, Guo P, Gallo JM. Pharmacodynamic-mediated effects of the angiogenesis inhibitor SU5416 on the tumor disposition of temozolomide in subcutaneous and intracerebral glioma xenograft models. J Pharmacol Exp Ther 2003;305:833–9.
25. Ansiaux R, Baudelet C, Jordan BF, et al. Mechanism of reoxygenation after antiangiogenic therapy using SU5416 and its importance for guiding combined antitumor therapy. Cancer Res 2006;66:9698–704.
26. Dickson PV, Hamner JB, Sims TL, et al. Bevacizumab-induced transient remodeling of the vasculature in neuroblastoma xenografts results in improved delivery and efficacy of systemically administered chemotherapy. Clin Cancer Res 2007;13:3942–50.
27. Kato T, Sato K, Kakinuma H, Matsuda Y (1994). Enhanced suppression of tumor growth by combination of angiogenesis inhibitor O-(chloroacetyl-carbamoyl)-fumagillol (TNP-470) and cytotoxic agents in mice. Cancer Res 1994;54:5143–7.
28. Fadnes HO, Reed RK, Aukland K. Interstitial fluid pressure in rats measured with a modified wick technique. Microvasc Res 1977;14:27–36.
29. Zhou Q, Guo P, Wang X, Nuthalapati S, Gallo JM. Preclinical pharmacokinetic and pharmacodynamic evaluation of metronomic and conventional temozolomide dosing regimens. J Pharmacol Exp Ther 2007;321:265–75.
30. Barrett PH, Bell BM, Cobelli C, et al. SAAM II: simulation, analysis, and modeling software for tracer and pharmacokinetic studies. Metabolism 1998;47:484–92.
31. Baluk P, Morikawa S, Haskell A, Mancuso M, McDonald DM. Abnormalities of basement membrane on blood vessels and endothelial sprouts in tumors. Am J Pathol 2003;163:1801–15.
32. Morikawa S, Baluk P, Kaidoh T, Haskell A, Jain RK, McDonald DM. Abnormalities in pericytes on blood vessels and endothelial sprouts in tumors. Am J Pathol 2002;160:985–1000.

**33.** Wong AL, Haroon ZA, Werner S, Dewhirst MW, Greenberg CS, Peters KG. Tie2 expression and phosphorylation in angiogenic and quiescent adult tissues. Circ Res 1997;81:567–74.

**34.** Holash J, Maisonpierre PC, Compton D, et al. Vessel cooption, regression, and growth in tumors mediated by angiopoietins and VEGF. Science 1999;284:1994–8.

**35.** Maisonpierre PC, Suri C, Jones PF, et al. Angiopoietin-2, a natural antagonist for Tie2 that disrupts *in vivo* angiogenesis. Science 1997;277:55–60.

**36.** Reiss Y, Machein MR, Plate KH. The role of angiopoietins during angiogenesis in gliomas. Brain Pathol 2005;15:311–7.

**37.** Tait CR, Jones PF. Angiopoietins in tumours: the angiogenic switch. J Pathol 2004;204:1–10.

**38.** Gallo JM, Vicini P, Orlansky A, et al. Pharmacokinetic model-predicted anticancer drug concentrations in human tumors. Clin Cancer Res 2004;10:8048–58.

**39.** Pietras K, Ostman A, Sjoquist M, et al. Inhibition of platelet-derived growth factor receptors reduces interstitial hypertension and increases transcapillary transport in tumors. Cancer Res 2001;61:2929–34.

**40.** Tong RT, Boucher Y, Kozin SV, Winkler F, Hicklin DJ, Jain RK. Vascular normalization by vascular endothelial growth factor receptor 2 blockade induces a pressure gradient across the vasculature and improves drug penetration in tumors. Cancer Res 2004;64:3731–6.

**41.** Ding H, Roncari L, Wu X, et al. Expression and hypoxic regulation of angiopoietins in human astrocytomas. Neuro-oncol 2001;3:1–10.

**42.** Zagzag D, Hooper A, Friedlander DR, et al. *In situ* expression of angiopoietins in astrocytomas identifies angiopoietin-2 as an early marker of tumor angiogenesis. Exp Neurol 1999;159:391–400.

**43.** Davis S, Aldrich TH, Jones PF, et al. Isolation of angiopoietin-1, a ligand for the TIE2 receptor, by secretion-trap expression cloning. Cell 1996;87:1161–9.

**44.** Kim I, Moon SO, Han CY, et al. The angiopoietin-tie2 system in coronary artery endothelium prevents oxidized low-density lipoprotein-induced apoptosis. Cardiovasc Res 2001;49:872–81.

## Correction: Article on Impact of Angiogenesis Inhibition by Sunitinib on Tumor Distribution of Temozolomide

In the article on impact of angiogenesis inhibition by sunitinib on tumor distribution of temozolomide in the March 1, 2008 issue of *Clinical Cancer Research*, the key in Fig. 1B was labeled incorrectly. The correct figure appears here.

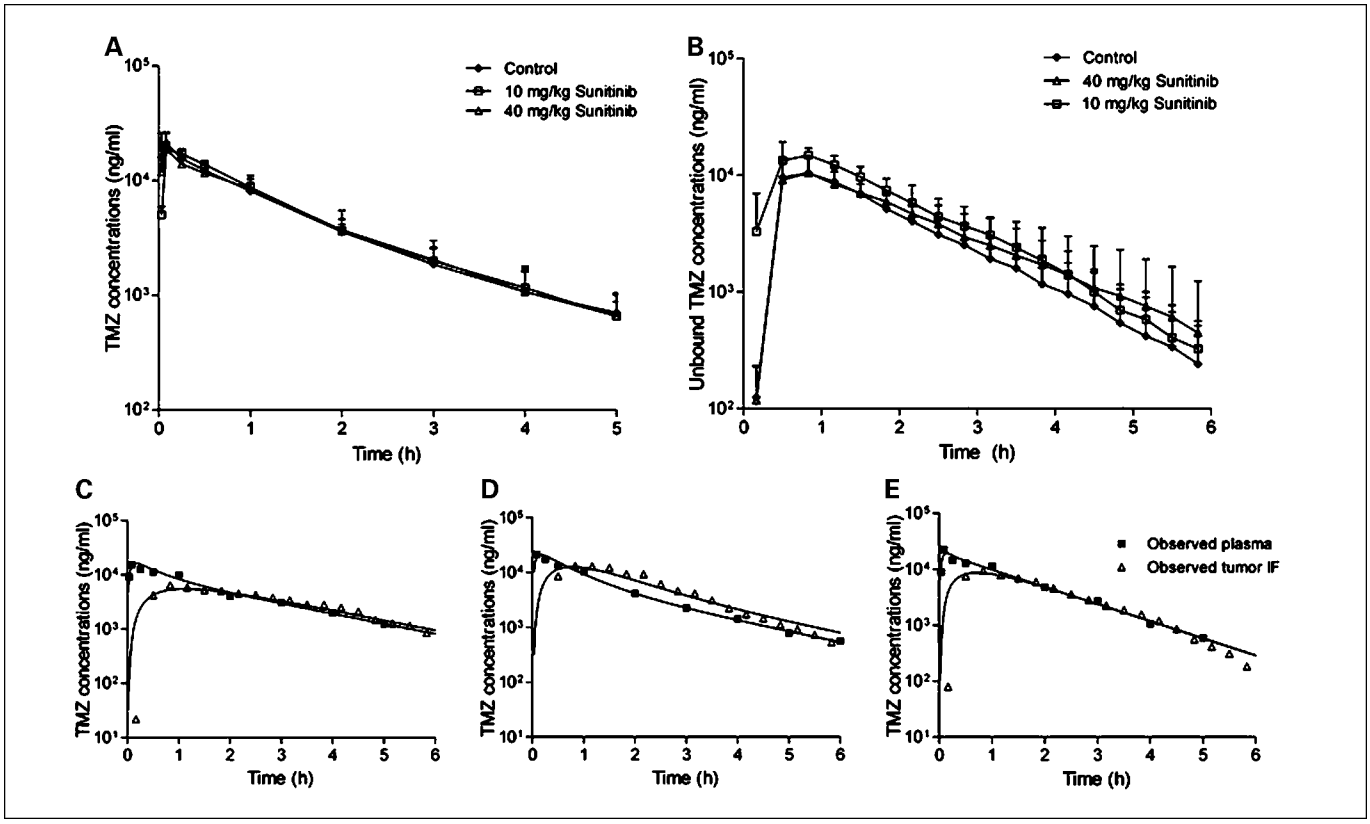


Zhou Q, Guo P, Gallo JM. Impact of Angiogenesis Inhibition by Sunitinib on Tumor Distribution of Temozolomide. Clin Cancer Res 2008;14:1540–49.


doi:10.1158/1078-0432.CCR-14-16-COR2

Clinical Cancer Research

# Impact of Angiogenesis Inhibition by Sunitinib on Tumor Distribution of Temozolomide

Qingyu Zhou, Ping Guo and James M. Gallo

*Clin Cancer Res* 2008;14:1540-1549.